CHEMISTRY OF MATERIALS
Article

Chem. Mater. **2010,** *22,* 4931–4938 4931
DOI:10.1021/cm101692a

Reversible Soft-Contact Lamination and Delamination for Non-Invasive Fabrication and Characterization of Bulk-Heterojunction and Bilayer Organic Solar Cells

Jong Bok Kim,[†] Stephanie Lee,[†] Michael F. Toney,[‡] Zhihua Chen,[§] Antonio Facchetti,[§] Youn Sang Kim,[∥] and Yueh-Lin Loo*,[†]

[†]*Department of Chemical and Biological Engineering, Princeton University, Princeton, New Jersey 08544,* [‡]*Stanford Synchrotron Radiation Lightsource, SLAC National Accelerator Laboratory, Menlo Park, California 94025,* [§]*Polyera Corporation, Skokie, Illinois 60077, and* [∥]*Department of Nano Science and Technology, Graduate School of Convergence Science and Technology, Seoul National University, Seoul 151-742, Korea*

Received June 17, 2010. Revised Manuscript Received July 26, 2010

Soft-contact lamination (ScL) provides a means to non-invasively establish electrical contact in organic solar cells. In contrast to the typical bottom-up fabrication approaches wherein active components are deposited sequentially in a layer-by-layer fashion, ScL allows individual functional layers to be separately deposited and optimized before these isolated components are brought together to complete the devices. Lamination and delamination of top electrodes to and from the active layer, respectively, are reversible and thus enables the characterization of the once-buried active layer after device processing and testing. ScL also enables the fabrication and characterization of bilayer organic solar cells comprising electron donors and electron acceptors that have comparable solubilities, the fabrication of which would not have been possible with the standard bottom-up approaches.

1. Introduction

The promise of low-cost, lightweight photovoltaics has fueled research in organic and polymer solar cells.[1,2] Indeed, in recent years, the efficiencies of organic and polymer-based solar cells have improved dramatically,[3−5] with Solamer holding the current record efficiency of 7.4%. The advances thus far can be attributed to the design and synthesis of new organic and polymer semiconductors having improved mobility,[6,7] smaller band gaps,[8,9] appropriate energy levels,[10] and increased solubility.[11] The processing and fabrication of organic solar cells, however, have largely remained unchanged. Borrowing from the established silicon community, transparent metal oxide conductors are first patterned via photolithography on glass or flexible substrates to produce bottom electrodes. The active layer is formed either by the deposition of a cosolution of the electron donor and electron acceptor to create a bulk-heterojunction structure, or by sequential deposition of the organic semiconductors to create a bilayer structure. The top electrode is then deposited directly on top of the active layer. While this bottom-up approach has generally yielded functional devices, the layer-by-layer sequential deposition approach presents several limitations. In the fabrication of organic solar cells with bilayer structures, for example, organic semiconductors soluble in similar solvents cannot be employed in a single cell, because the solution deposition of one species on top of the other necessarily induces solvent damage of the underlying organic semiconductor. Individually cross-linked layers have thus been employed to avoid dissolution during subsequent exposures to solvents.[12] Furthermore, the buried interfaces at which charge separation and transfer occur in organic solar cells, including the electron donor/electron acceptor interface in bilayer structures, as well as the active layer/electrode interface in bulk-heterojunction structures, are not directly accessible for characterization after device fabrication is complete. Recent attempts to

*Author to whom correspondence should be addressed. Tel.: +1-609-258-9091. Fax: +1-609-258-0211. E-mail: lloo@princeton.edu.

(1) Kippelen, B.; Bredas, J.-L. *Energy Environ. Sci.* **2009**, *2*, 251.
(2) Hoppe, H.; Sariciftci, N. S. *Adv. Polym. Sci.* **2008**, *214*, 1.
(3) Park, S. H.; Roy, A.; Beaupre, S.; Cho, S.; Coates, N.; Moon, J. S.; Moses, D.; Leclerc, M.; Lee, K.; Heeger, A. J. *Nat. Photonics* **2009**, *3*, 297.
(4) Liang, Y.; Xu, Z.; Xia, J.; Tsai, S.-T.; Wu, Y.; Li, G.; Ray, C.; Yu, L. *Adv. Mater.* **2010**, *22*, E135.
(5) Ameri, T.; Dennler, G.; Lungenschmied, C.; Brabec, C. J. *Energy Environ. Sci.* **2009**, *2*, 347.
(6) Wong, W.-Y.; Wang, X.-Z.; He, Z.; Djurisic, A. B.; Yip, C.-T.; Cheung, K.-Y.; Wang, H.; Mak, C. S. K.; Chan, W.-K. *Nat. Mater.* **2007**, *6*, 521.
(7) Li, Y.; Zou, Y. *Adv. Mater.* **2008**, *20*, 2952.
(8) Thompson, B. C.; Frechet, J. M. J. *Angew. Chem., Int. Ed.* **2008**, *47*, 58.
(9) Winder, C.; Sariciftci, N. S. *J. Mater. Chem.* **2004**, *14*, 1077.
(10) Ross, R. B.; Cardona, C. M.; Guldi, D. M.; Sankaranarayanan, S. G.; Reese, M. O.; Kopidakis, N.; Peet, J.; Walker, B.; Bazan, G. C.; Keuren, E. V.; Holloway, B. C.; Drees, M. *Nat. Mater.* **2009**, *8*, 208.
(11) Troshin, P. A.; Hoppe, H.; Renz, J.; Egginger, M.; Mayorova, J. Y.; Goryachev, A. E.; Peregudov, A. S.; Lyubovskaya, R. N.; Gobsch, G.; Sariciftci, N. S.; Razumov, V. F. *Adv. Func. Mater.* **2009**, *19*, 779.
(12) Kim, B. J.; Miyamoto, Y.; Ma, B.; Frechet, J. M. J. *Adv. Funct. Mater.* **2009**, *19*, 2273.

Published on Web 08/11/2010

examine these interfaces include spectroscopic characterization of a polymer thin film resembling that of a bulk-heterojunction active layer after delamination from model silicon dioxide substrates.[13] While the use of such model substrates allows the delamination and subsequent characterization of the once-buried interface, the characterized interface is not necessarily representative of the actual charge transfer interface in functional devices. A non-invasive approach that allows the direct elucidation of buried charge separation and charge transfer interfaces in organic solar cells is thus still critically needed.

In this paper, we exploit the non-destructive nature of soft-contact lamination (ScL) to construct organic and polymer solar cells for testing and then non-invasively deconstructing them for subsequent characterization of the once-buried active layers. The use of ScL circumvents the need for bottom-up, sequential deposition of functional materials for fabricating organic solar cells; individual components are separately processed and optimized before they are brought together into electrical contact in the final steps of fabrication. Physical contact occurs at ambient temperatures and pressures, so this process does not present adverse effects to mechanically- and chemically-fragile organics. ScL was first introduced to establish non-invasive electrical contact in thin-film transistors;[14−16] source and drain electrodes that were laminated against the organic semiconductor channel exhibit markedly reduced contact resistance, compared to those directly evaporated through a stencil mask. Metal electrodes have also been physically contacted against organics to create light-emitting diodes.[17,18] Such laminated devices exhibit more homogeneous electrical contact and reduced pinhole defects. Building upon these reports, the construction of organic solar cells by physical lamination of top electrodes in bulk-heterojunction devices has been demonstrated.[19−22] Here, we exploit one of the unique attributes of ScL by non-invasively delaminating the once-laminated components of organic solar cells after device testing to elucidate the structural development at the once-buried charge transfer interface.

2. Experimental Section

Organic solar cells with bulk-heterojunction structures and bilayer structures were fabricated via ScL. Lamination in bulk-heterojunction organic solar cells occurred at the charge-transfer interface between the top electrodes and the active layer. Lamination in bilayer organic solar cells occurred at the organic/organic interface between the electron donor and the electron acceptor. Starting with the inverted device architecture that exhibits unprecedented air stability,[23] Figure 1 schematically illustrates the lamination process for constructing bulk-heterojunction organic solar cells. The ScL process calls for two parts: a transparent substrate that supports the bottom electrodes onto which the active layer is deposited, and an independent elastomeric substrate that supports the top electrodes. The bottom substrate is prepared by first patterning indium tin oxide (ITO) electrodes on glass or plastic via photolithography. Unlike devices constructed in the conventional architecture, ITO electrodes serve as cathodes to collect electrons in our devices. Onto the patterned ITO electrodes, we deposit a 1 wt % solution comprising titanium isopropoxide ($Ti[OCH](CH_3)_2]_4$, Aldrich, 99.999% purity) in isopropyl alcohol. Hydrolysis of the precursor at room temperature for 1 h and subsequent annealing at 170 °C for 10 min yields a 30-nm-thick titania layer.[23−25] This titania layer serves two roles: it acts as a buffer layer to smooth out the rough ITO surface and it also blocks hole transport, effectively increasing the rectification ratio of our devices. A 180-nm-thick film comprising a blend having an equimass ratio of poly(3-hexylthiophene) (P3HT, Merck Chemicals, Ltd.) and [6,6]-phenyl-C_{61}-butyric acid methyl ester (PCBM, American Dye Source, Inc.), as the electron donor and electron acceptor, respectively, makes up the active layer. The deposition of gold contact pads onto which the top electrodes will subsequently laminate against completes the fabrication of the bottom portion of the device.

The top substrate consists of gold electrodes, patterned by direct evaporation through a stencil mask, on cross-linked poly(dimethyl siloxane) (PDMS). Given the inverted architecture we have chosen, the top electrode no longer must be aluminum. We have thus opted for gold as the high-work-function anode to collect holes during device operation. Prior to gold evaporation, the PDMS substrate is selectively treated by UV/ozone through the same stencil mask that is used to define the top electrodes. This process converts the exposed regions of PDMS to a silica-like surface and thus decreases thermal expansion and shrinkage during evaporation,[26,27] effectively eliminating cracks in the subsequently deposited gold electrodes. Silver electrodes have also been fabricated on the top substrate in an analogous fashion. When oxidized, silver oxide exhibits a comparable work function to gold;[28−30] we have thus also been able to employ oxidized silver as anodes in our inverted organic solar cells to collect holes.

With the fabrication of the bottom and top substrates complete, these two portions are gently brought together at room

(13) Germack, D. S.; Chan, C. K.; Hamadani, B. H.; Richter, L. J.; Fischer, D. A.; Gundlach, D. J.; DeLongchamp, D. M. *Appl. Phys. Lett*. **2009**, *94*, 233303.
(14) Zaumseil, J.; Baldwin, K. W.; Rogers, J. A. *J. Appl. Phys*. **2003**, *93*, 6117.
(15) Loo, Y.-L.; Someya, T.; Baldwin, K. W.; Bao, Z.; Ho, P.; Dodabalapur, A.; Katz, H. E.; Rogers, J. A. *Proc. Natl. Acad. Sci. U.S.A*. **2002**, *99*, 10252.
(16) Zaumseil, J.; Someya, T.; Bao, Z.; Loo, Y.-L.; Cirelli, R.; Rogers, J. A. *Appl. Phys. Lett*. **2003**, *82*, 793.
(17) Lee, T.-W.; Zaumseil, J.; Bao, Z.; Hsu, J. W. P.; Rogers, J. A. *Proc. Natl. Acad. Sci. U.S.A*. **2004**, *101*, 429.
(18) Guo, T.-F.; Pyo, S.; Chang, S.-C.; Yang, Y. *Adv. Funct. Mater*. **2001**, *11*, 339.
(19) Granstrom, M.; Petritsch, K.; Arias, A. C.; Lux, A.; Andersson, M. R.; Friend, R. H. *Nature* **1998**, *395*, 257.
(20) Huang, J.; Li, G.; Yang, Y. *Adv. Mater*. **2008**, *20*, 415.
(21) Kim, J.; Khang, D.-Y.; Kim, J.-H.; Lee, H. H. *Appl. Phys. Lett*. **2008**, *92*, 133307.
(22) Gadisa, A.; Tvingstedt, K.; Admassie, S.; Lindell, L.; Crispin, X.; Andersson, M. R.; Salaneck, W. R.; Inganas, O. *Synth. Met*. **2006**, *156*, 1102.
(23) Kim, C. S.; Lee, S. S.; Gomez, E. D.; Kim, J. B.; Loo, Y.-L. *Appl. Phys. Lett*. **2009**, *94*, 113302.
(24) Kim, J. Y.; Kim, S. H.; Lee, H.-H.; Lee, K.; Ma, W.; Gong, X.; Heeger, A. J. *Adv. Mater*. **2006**, *18*, 572.
(25) Kim, C. S.; Tinker, L. L.; DiSalle, B. F.; Gomez, E. D.; Lee, S.; Bernhard, S.; Loo, Y.-L. *Adv. Mater*. **2009**, *21*, 3110.
(26) Kim, J. B.; Choi, C. J.; Park, J. S.; Jo, S. J.; Hwang, B. H.; Jo, M. K.; Kang, D.; Lee, S. J.; Kim, Y. S.; Baik, H. K. *Adv. Mater*. **2008**, *20*, 3073.
(27) Efimenko, K.; Wallace, W. E.; Genzer, J. *J. Colloid Interface Sci*. **2002**, *254*, 306.
(28) Choi, H. W.; Kim, S. Y.; Kim, K.-B.; Tak, Y.-H.; Lee, J.-L. *Appl. Phys. Lett*. **2005**, *86*, 012104.
(29) Kim, J. B.; Kim, C. S.; Kim, Y. S.; Loo, Y.-L. *Appl. Phys. Lett*. **2009**, *95*, 183301.
(30) Kim, C. S.; Kim, J. B.; Kim, Y. S.; Lee, S. S.; Loo, Y.-L. *Org. Electron*. **2009**, *10*, 1483.

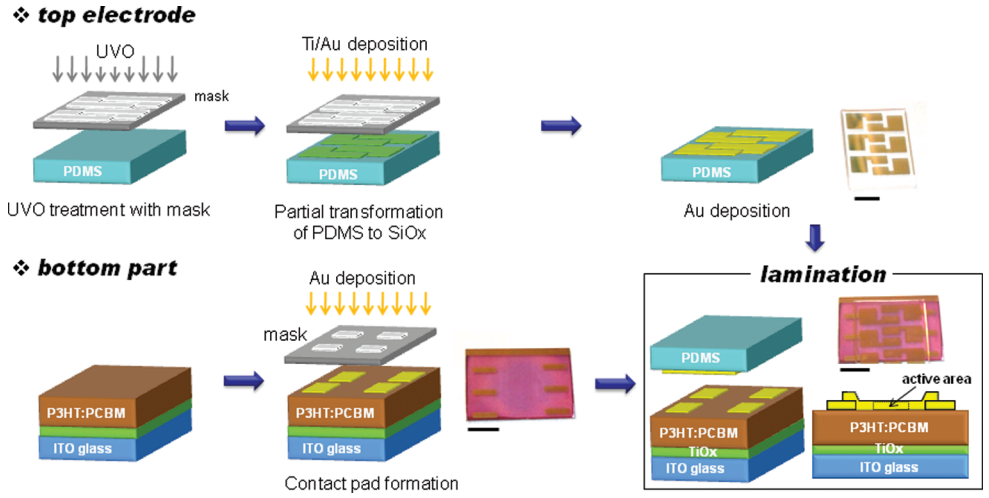

Figure 1. Schematic illustration of the soft-contact lamination (ScL) process employed to fabricate organic solar cells. To create the top electrode, poly(dimethyl siloxane) (PDMS) is selectively treated by UV/ozone through a stencil mask, followed by Ti/Au deposition using the same stencil mask. The bottom portion of the device consists of prepatterned ITO on glass, onto which TiO_x, P3HT:PCBM, and the contact pads are deposited. Physical lamination completes device fabrication. Photographs of the top electrode, the bottom portion, and the device after lamination are included; scale bars correspond to 10 mm.

temperature. Physical contact is initiated from one corner of the PDMS substrate and the pad is gently laid down against the active layer to avoid trapping of air bubbles at the laminated interface. No external pressure is required to establish contact. The top PDMS substrate generally supports five sets of electrodes; lamination against the bottom substrate thus yields an array of five inverted organic solar cells. The active area of each laminated organic solar cell is 0.18 cm^2.

We also constructed bilayer organic solar cells by laminating the polymer electron donor against the electron acceptor. We have chosen to demonstrate this concept with two pairs of electron donor and electron acceptor: the first pair comprises of P3HT and PCBM while the second pair consists of P3HT and a polymer electron acceptor[31] of poly{[*N*,*N*′-bis(2-octyldodecyl)-naphthalene-1,4,5,8-bis(dicarboximide)-2,6-diyl]-alt-5,5′-(2,2′-bithiophene)}, or P(NDI2OD-T2). Because P3HT and PCBM (as well as P3HT and P(NDI2OD-T2)) are soluble in solvents with comparable polarities, bilayer organic solar cells comprising these material combinations cannot be constructed via sequential deposition of the organic semiconductors directly. More specifically, the solvent that is used to deposit the top layer will necessarily erode the underlying organic semiconductor.

Device testing was carried out with a Keithley Model 2400 source measurement unit under AM 1.5G 100mW/cm^2 illumination. Before testing, each device was illuminated for 10 min to fill shallow electron traps in the titania electron transport layer.[23] Current density−voltage ($J-V$) characteristics were acquired 2 days after device fabrication in bulk-heterojunction solar cells and immediately after device fabrication in bilayer organic solar cells. All the devices were fabricated and tested in air.

Structural characterization of the once-buried bulk-heterojunction active layer was carried out by grazing-incidence X-ray diffraction (GIXD), using Beamline 11-3 at the Stanford Synchrotron Radiation Lightsource. An incident angle of 0.11° was employed and an area detector was used to acquire scattered X-rays. The X-ray energy was 12.7 eV. UV−vis−NIR and external quantum efficiency (EQE) spectra of P3HT/PCBM and P3HT/P(NDI2OD-T2) bilayers were acquired using an Agilent Model 8453 spectrophotometer with 1 nm resolution and a Newport Monochrometer 74100 system, respectively.

(31) Yan, H.; Chen, Z.; Zheng, Y.; Newman, C.; Quinn, J. R.; Dotz, F.; Kastler, M.; Facchetti, A. *Nature* **2009**, *457*, 679.

3. Results and Discussion

Figures 2a and 2b show the current density−voltage ($J-V$) characteristics of one such organic solar cell with several different laminated top electrodes in the dark and under illumination. Specifically, we first employed an array of gold electrodes on an active layer that had been previously annealed at 170 °C to complete the organic solar cells. The $J-V$ characteristics of a representative device are illustrated with open squares. Of the five devices tested, they all show reasonable rectification ratios (on the order of 10^3) when the diodes operate in the dark. Under illumination, the same devices exhibit an average open-circuit voltage (V_{oc}) of -0.56 ± 0.01 V, an average short-circuit current density (J_{sc}) of 6.96 ± 0.62 mA/cm^2, and an average fill factor of 0.53 ± 0.03, resulting in an average efficiency of $2.03\% \pm 0.29\%$. These extracted photovoltaic characteristics are comparable to those extracted from similarly fabricated devices with evaporated gold top electrodes. Because we are collecting electrons at the ITO cathode and holes at the gold anode during operation of our inverted solar cells, power generation occurs in the second quadrant of the $J-V$ graph with a negative V_{oc} and positive J_{sc}.[29] For comparison, devices constructed in the conventional architecture exhibit power generation curves in the fourth quadrant: a positive V_{oc} and a negative J_{sc} are recorded. To test the robustness of our lamination process, we removed the top PDMS substrate supporting the first set of gold electrodes and replaced it with a second array of gold electrodes; the $J-V$ characteristics of the solar cell comprising the same active layer but a newly laminated gold electrode are shown as open circles in Figure 2. The diode characteristics in the dark are comparable to those of the same device with the prior set of gold electrodes. Testing the same five devices under illumination yielded an average V_{oc} value of -0.56 ± 0.01 V,

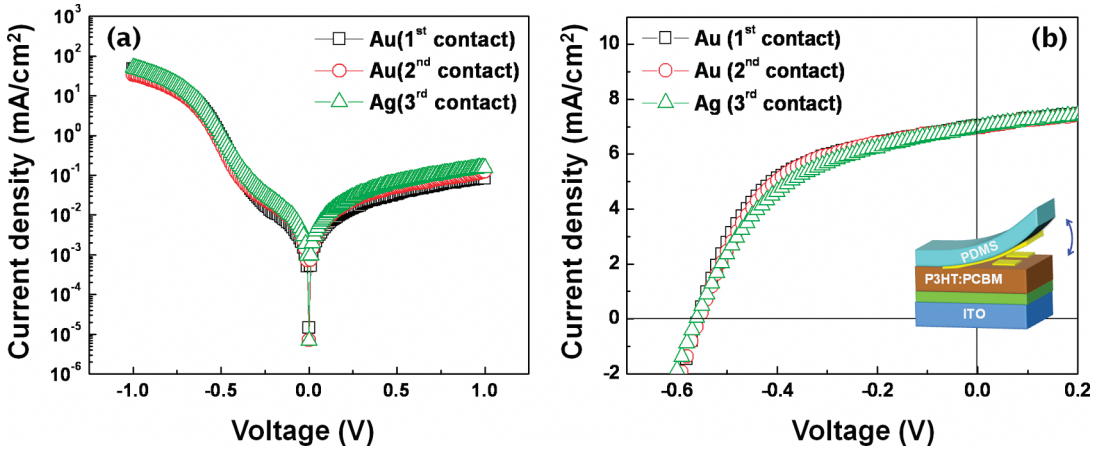

Figure 2. $J-V$ characteristics of inverted solar cells with several different laminated top electrodes on the same active layer (a) in the dark and (b) under illumination (100 mW/cm^2). The active layer was thermally annealed at 170 °C for 1 min prior to lamination. After testing, the gold electrodes were removed and replaced with new sets of gold and oxidized silver electrodes for further testing.

an average J_{sc} value of 6.93 ± 0.63 mA/cm^2, and an average fill factor of 0.53 ± 0.01. Accordingly, the average efficiency is 2.07% ± 0.18%. The fact that the device characteristics are unchanged with the replacement of laminated electrodes is a strong indication that we have reestablished efficient electrical contact; the $J-V$ characteristics therefore are a reflection of the active layer and are not limited by contact effects at the active layer/top electrode interface. Finally, the second array of gold electrodes was removed and replaced with an array of oxidized silver electrodes; the $J-V$ characteristics associated with the same device, but now with an oxidized silver electrode, are shown as open triangles in Figure 2. The diode characteristics obtained in the dark are again largely comparable with the device tested prior. Repeated testing of the five devices under illumination resulted in an average V_{oc} value of −0.56 ± 0.01 V, an average J_{sc} value of 7.11 ± 0.33 mA/cm^2, an average fill factor of 0.51 ± 0.03, and an average efficiency of 2.02% ± 0.26%. The $J-V$ characteristics are comparable to those obtained on the devices when they were laminated with gold electrodes, since oxidized silver has a work function that is comparable to that of gold. The results summarized in Figure 2 indicate ScL to be a robust method of establishing efficient electrical contact to organic layers in solar cells. Multiple top electrodes can be laminated reversibly against the same active layer for testing. The modularity of this process thus affords new opportunities for engineering the charge-transfer interface between the organic active layer and the top electrodes. Specifically, with laminated organic solar cells, we are currently investigating how the presence of adlayers on the top electrode influences device characteristics. These experiments—previously not possible with devices constructed in the bottom-up approach—are uniquely enabled by the ability to laminate, nondestructively remove, and then subsequently relaminate top electrodes to the same active layer.

The ability to nondestructively remove the top electrode after device fabrication and testing has enabled us to examine the morphological development of the once-buried active layer. Because the active layer has been difficult to access, improvements in solar cell performance observed with thermal annealing after top electrode deposition have frequently been attributed to increases in crystallinity of the organic semiconductors.[32,33] This inference is based on structural characterization of thin organic films that have been subjected to processing histories comparable to those of active layers in solar cells, but in the absence of the top electrodes. Given that the structure of active layers, and, hence, the device performance, can be highly dependent on the details of processing,[34,35] morphological characteristics of thin films annealed in the absence of the top electrode may not be representative of those in actual devices, where the active layers are frequently annealed after electrode deposition.

Given the versatility of ScL, we have been able to elucidate the structure of the active layer in functional organic solar cells directly. In Figure 3a, we quantify the increases in J_{sc} (open squares; left y-axis) and, accordingly, device efficiency (open circles; right y-axis) of P3HT:PCBM inverted bulk-heterojunction solar cells with post-device fabrication thermal annealing. In the absence of thermal annealing, the J_{sc} value averages 1.26 ± 0.02 mA/cm^2 for five devices. Subjecting similarly prepared devices to thermal annealing after top electrode deposition progressively increases the J_{sc} value; devices that were thermally annealed at 170 °C exhibit an average J_{sc} value of 7.81 ± 0.37 mA/cm^2. This increase in J_{sc} is reflected in a concomitant increase in device efficiency; the average device efficiency increases from 0.21% ± 0.02% for unannealed devices to 1.39% ± 0.05% for

(32) Campoy-Quiles, M.; Ferenczi, T.; Agostinelli, T.; Etchegoin, P. G.; Kim, Y.; Anthopoulos, T. D.; Stavrinou, P. N.; Bradley, D. D. C.; Nelson, J. *Nat. Mater.* **2008**, *7*, 158.
(33) Vanlaeke, P.; Swinnen, A.; Haeldermans, I.; Vanhoyland, G.; Aernouts, T.; Cheyns, D.; Deibel, C.; D'Haen, J.; Heremans, P.; Poortmans, J.; Manca, J. V. *Sol. Energy Mater. Sol. Cells* **2006**, *90*, 2150.
(34) McNeill, C. R.; Halls, J. J. M.; Wilson, R.; Whiting, G. L.; Berkebile, S.; Ramsey, M. G.; Friend, R. H.; Greenham, N. C. *Adv. Funct. Mater.* **2008**, *18*, 2309.
(35) Li, G.; Shrotriya, V.; Yao, Y.; Yang, Y. *J. Appl. Phys.* **2005**, *98*, 043704.

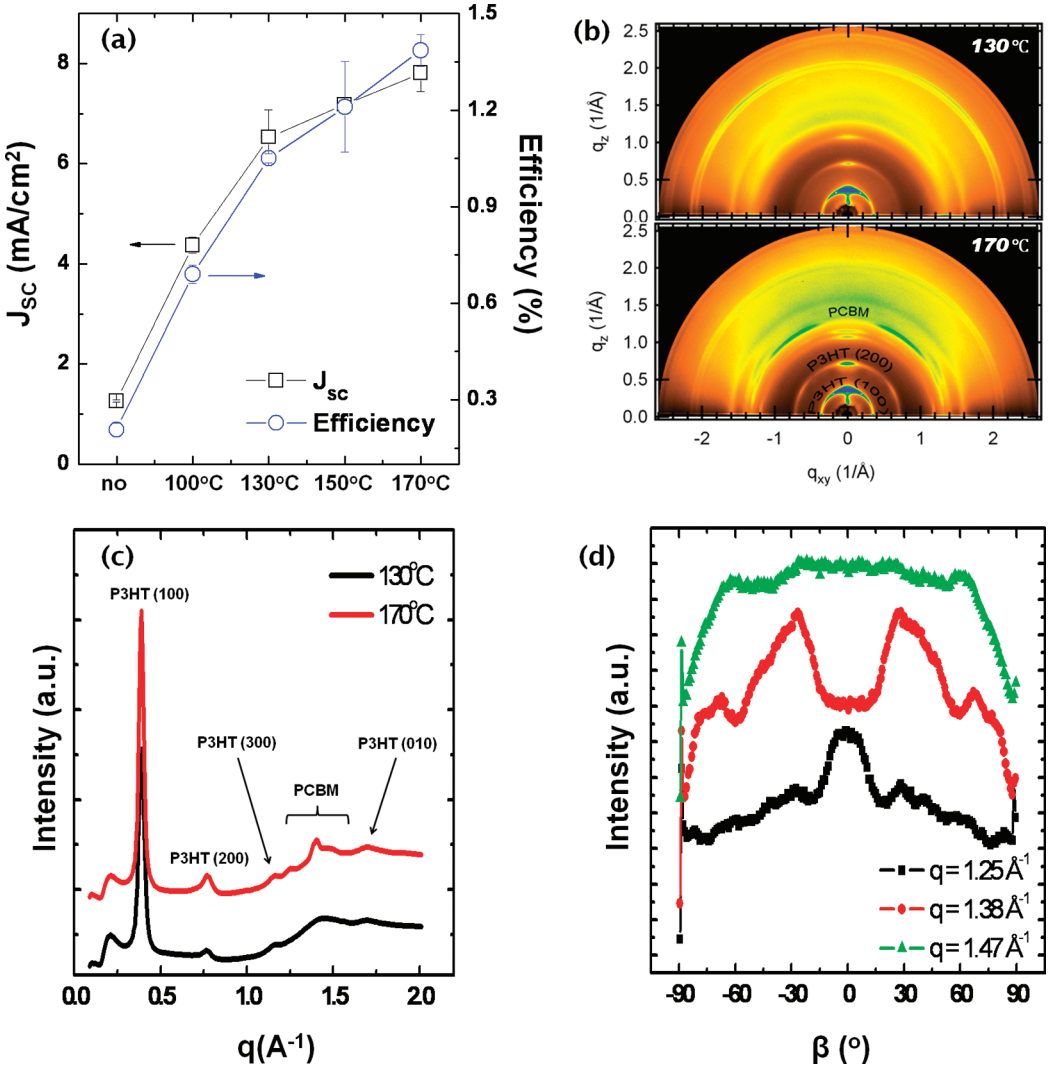

Figure 3. (a) Device characteristics (J_{sc}, efficiency) of P3HT:PCBM inverted polymer solar cells that were annealed at different temperatures for 1 min after top electrode lamination; (b) grazing-incidence X-ray diffraction (GIXD) patterns acquired on once-buried active layers in devices that were annealed at 130 and 170 °C; (c) one-dimensional X-ray profiles generated by azimuthally averaging across the X-ray patterns shown in panel (b); (d) azimuthal line traces of the PCBM reflections generated from the X-ray pattern of the active layer that was annealed at 170 °C.

devices that were annealed at 170 °C after top electrode deposition. Thermal annealing after top electrode deposition always resulted in increases in J_{sc} and device efficiency; this trend is observed for devices both with laminated and with directly evaporated top gold electrodes. While directly evaporated top electrodes cannot be easily removed after device testing without inducing physical damage to the active layer, the laminated electrodes can be peeled away non-invasively, to reveal the once-buried active layer for subsequent structural characterization.

The top and bottom portions of Figure 3b show GIXD images acquired on active layers after removal of laminated top electrodes from organic solar cells that had been thermally annealed at 130 and 170 °C, respectively. We have labeled the lamella or (h00) reflections of P3HT at q (scattering vector) = 0.37 $Å^{-1}$, 0.74 $Å^{-1}$, and 1.11 $Å^{-1}$ for clarity. Also labeled is the broad reflection at 1.4 $Å^{-1}$ that is associated with PCBM. The P3HT (h00) reflections are more intense at the meridian compared to the equator, which is an indication that P3HT crystals are preferentially oriented with the (h00) planes parallel to the substrate. Given the crystal structure of P3HT, this preferential orientation necessitates that π-stacking of P3HT in the active layers is largely in-plane. Comparing the X-ray diffraction (XRD) patterns reveals that the P3HT (h00) reflections are significantly stronger and better defined for the device annealed at 170 °C. Even more striking is the difference in the PCBM scattering. The diffraction pattern acquired on the active layer when the device is subjected to thermal annealing at 130 °C reveals a broad and diffuse PCBM reflection, implying the amorphous nature of PCBM. This reflection sharpens significantly in the diffraction pattern acquired on the active layer annealed at 170 °C, suggesting that PCBM is now at least partially crystalline. Furthermore, we observe that the intensities of the sharper PCBM reflections are nonuniform azimuthally; enhanced intensities off the meridian show that PCBM crystallites are preferentially oriented when the device is annealed at 170 °C.

To compare the P3HT and PCBM microstructures and crystallinities between the two active layers, we

azimuthally averaged across the X-ray patterns to obtain the one-dimensional X-ray profiles shown in Figure 3c. The reflections associated with P3HT and PCBM are labeled for clarity. The diffraction profile acquired on the active layer that was annealed at 170 °C reveals significantly stronger and more pronounced P3HT (h00) reflections (at 0.37, 0.74, and 1.11 $Å^{-1}$), compared to that of the active layer annealed at 130 °C. While our GIXD data do not allow the construction of complete pole figures or the comparison of total integrated intensities that is necessary for accurate assessment of cyrstallinity, the data in Figure 3c do suggest that P3HT is more crystalline when the active layer is annealed at 170 °C. In particular, this conclusion is supported by the fact that the P3HT (010) reflection in the X-ray profile extracted from the active layer annealed at 170 °C is much more prominent than that for the active layer annealed at 130 °C. Perhaps more surprising is the difference in PCBM crystallinity with annealing temperatures. The X-ray scan acquired on the active layer annealed at 130 °C reveals a broad reflection centered at 1.4 $Å^{-1}$ that is characteristic of amorphous PCBM. Annealing the active layer at 170 °C sharpens the PCBM reflections significantly. We observe three reflections that are associated with the crystal structure of PCBM. These appear at 1.25, 1.38, and 1.47 $Å^{-1}$.

In addition to enhanced crystallinity of both P3HT and PCBM, the X-ray pattern of the active layer annealed at 170 °C in Figure 3b reveals azimuthal variations in intensity associated with the PCBM reflections showing that the PCBM is preferentially oriented. Such preferential orientation of PCBM within thin-film blends of P3HT and PCBM has only been observed in one other scenario, where the blend is thermally annealed on poly(ethylene dioxythiophene) templated on poly(styrene sulfonic acid), PEDOT-PSS.[36,37] To quantify the orientation of PCBM, we show in Figure 3d the azimuthal scans, averaged over 0.05 $Å^{-1}$, of the XRD pattern of the active layer annealed at 170 °C, taken at a constant q_{xy} of 1.25 $Å^{-1}$ (black trace) and 1.38 $Å^{-1}$ (red trace) and 1.47 $Å^{-1}$ (green trace). The azimuthal angle (β) is defined to be 0° at the meridian and 90° at the equator. We observe that the azimuthal profile of the PCBM peak at 1.25 A^{-1} is near $\beta = 0°$, suggesting that these PCBM planes (crystal structure to be determined) are oriented approximately parallel to the substrate. The fact that PCBM is preferentially oriented within thin films comprising P3HT and PCBM could stem from confinement effects that are due to the presence of the top electrode during thermal annealing.[38]

Recent attempts to make bilayer devices comprising P3HT and PCBM involve cross-linking P3HT prior to the deposition of PCBM.[12] With ScL, the electron donor can be deposited on the top elastomeric substrate while the electron acceptor is deposited on the bottom substrate before the two portions are brought into contact; chemical derivatization of the organic semiconductors to impart physical integrity is not necessary. Figure 4a contains the illuminated $J-V$ characteristics of laminated bilayer organic solar cells comprising a P3HT and a 65-nm-thick PCBM layer that is directly spin-coated on the titania electron transport layer. P3HT of varying thickness (ranging from 120 nm to 400 nm) is first transferred onto elastomeric substrates with predeposited gold top electrodes, per previously published procedures,[39,40] and then laminated against the electron acceptor to complete the organic solar cells. Specifically, P3HT is first spin-coated from chlorobenzene on UV/ozone-treated glass. An elastomeric substrate, with evaporated top gold electrodes, is then brought into contact with P3HT and the entire assembly is soaked in water for 5 min. During immersion, water selectively wicks into the P3HT/glass interface, causing delamination of P3HT from the glass substrate and its transfer onto the elastomeric substrate. In Figure 4a, we observe that increasing the P3HT thickness from 120 nm to 160 nm increases the device J_{sc} value from 0.43 mA/cm^2 to 0.65 mA/cm^2. This increase in device J_{sc} is possibly due to enhanced light absorption with a thicker P3HT film. Further increasing the thickness of P3HT, however, results in decreases in device J_{sc}, first to 0.35 mA/cm^2 at 230 nm P3HT and then to 0.21 mA/cm^2 at 400 nm P3HT. This decrease in device J_{sc} is attributed to increases in the internal resistance of the device, because of the limited hole mobility of P3HT.[41] Furthermore, the overall thicknesses of P3HT are now significantly larger than the exciton diffusion length, so charge separation efficiency is dramatically reduced. There therefore exists an optimal thickness for P3HT in inverted bilayer organic solar cells where the device characteristics are maximized. Quantification of the fill factor indicates the efficiency with which our devices operate. Our laminated inverted bilayer devices uniformly exhibit fill factors that are greater than 0.4, indicating efficient electrical contact at the laminated charge separation interface.

The construction of bilayer organic solar cells by lamination is not limited to P3HT and PCBM. We have also successfully built inverted bilayer polymer−polymer solar cells comprised of P3HT as the electron donor and P(NDI2OD-T2)[31] as the electron acceptor by lamination across the electron donor/electron acceptor interface. Figure 4b contains the $J-V$ characteristics under light illumination of P3HT/P(NDI2OD-T2) bilayer polymer solar cells at varying P(NDI2OD-T2) thickness; the P3HT layer thickness is kept constant at 230 nm for this experiment. When the P(NDI2OD-T2) layer is thin, the shunt resistance of the device is low, as manifested by the low fill factor exhibited by devices composed of P(NDI2OD-T2) < 75 nm thick. When the P(NDI2OD-T2)

(36) Woo, C. H.; Thompson, B. C.; Kim, B. J.; Toney, M. F.; Frechet, J. M. J. *J. Am. Chem. Soc.* **2008**, *130*, 16324.
(37) Gomez, E. D.; Barteau, K. P.; Wang, H.; Guan, Z. L.; Kahn, A.; Schwartz, J.; Toney, M. F.; Loo, Y.-L. Unpublished work.
(38) Peumans, P.; Uchida, S.; Forrest, S. R. *Nature* **2003**, *425*, 158.
(39) Ferenczi, T. A. M.; Nelson, J.; Belton, C.; Ballantyne, A. M.; Campoy-Quiles, M.; Braun, F. M.; Bradley, D. D. C. *J. Phys.: Condens. Matter* **2008**, *20*, 475203.
(40) Yim, K.-H.; Zheng, Z.; Liang, Z.; Friend, R. H.; Huck, W. T. S.; Kim, J.-S. *Adv. Funct. Mater.* **2008**, *18*, 1012.
(41) Goh, C.; Kline, R. J.; McGehee, M. D.; Kadnikova, E. N.; Frechet, J. M. J. *Appl. Phys. Lett.* **2005**, *86*, 122110.

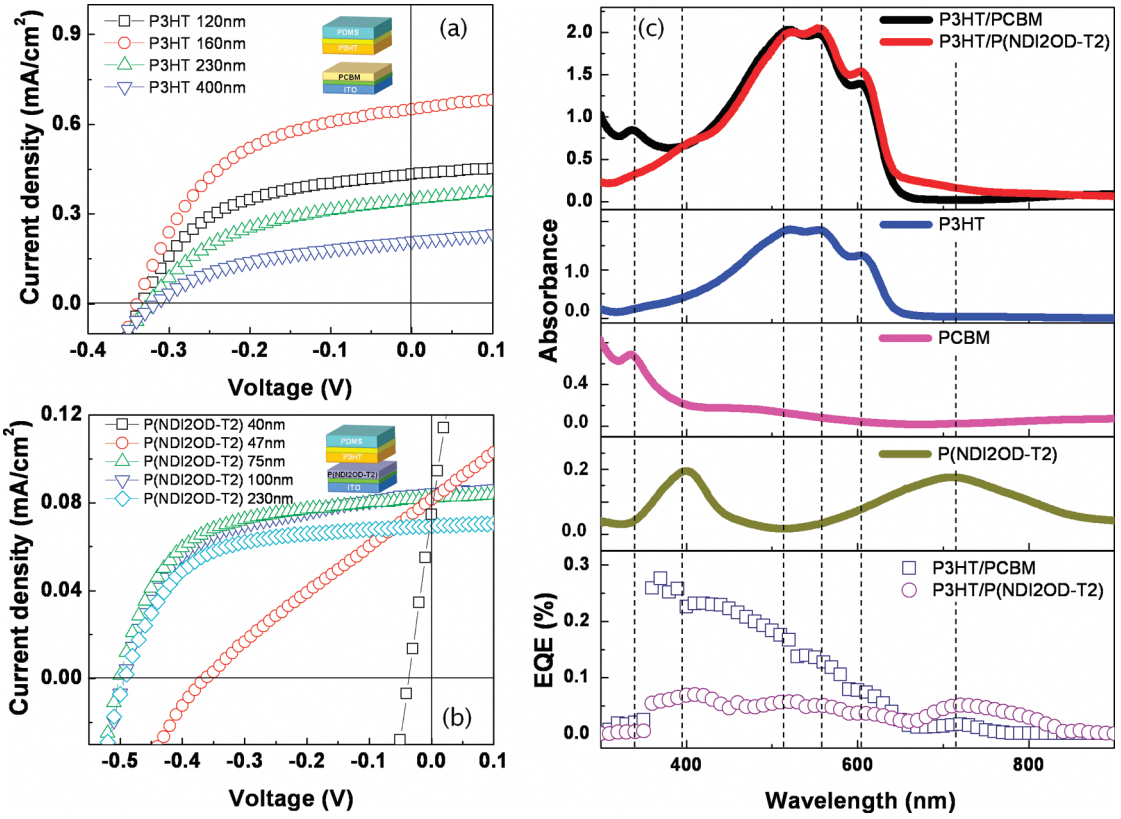

Figure 4. $J-V$ characteristics of laminated (a) P3HT/PCBM and (b) P3HT/P(NDI2OD-T2) bilayer organic solar cells with varying layer thicknesses. In panel (a), the PCBM layer thickness was kept constant at 65 nm. In panel (b), the P3HT layer thickness was kept constant at 230 nm. (c) From top to bottom: UV−vis−NIR spectra of bilayers of P3HT/PCBM (black; 230 and 65 nm, respectively) and P3HT/P(NDI2OD-T2) (red; 230 and 75 nm, respectively); and the spectra of the individual layers prior to lamination. Bottom graph consists of EQE spectra of laminated bilayer P3HT/PCBM (blue squares) and P3HT/P(NDI2OD-T2) (purple circles) polymer solar cells, whose device characteristics are represented in green triangles in panels (a) and (b), and whose UV−vis spectra of active layers are shown in the top portion of the figure.

layer is 75−100 nm, we observe decent device characteristics, with fill factors of >0.55. Further increasing the P(NDI2OD-T2) layer thickness, however, results in reducing the device J_{sc} value from 0.082 mA/cm^2 to 0.069 mA/cm^2, because of an increase in the internal resistance of the P(NDI2OD-T2) layer.

The top graph of Figure 4c contains the UV−vis−NIR absorption spectra of bilayers of P3HT/PCBM (230 and 65 nm, respectively) and P3HT/P(NDI2OD-T2) (230 and 75 nm, respectively). These layer thicknesses were chosen to simulate the active layers whose device characteristics are shown as green triangles in Figures 4a and 4b. The UV−vis−NIR spectra of the individual layers prior to lamination are also presented in Figure 4c, for the sake of comparison. We observe that the UV−vis−NIR spectra of the bilayers seem largely similar to that of P3HT, since P3HT is more efficient at absorbing light, compared to the electron acceptors we work with. Comparing the UV−vis−NIR spectra of the bilayers suggest that the efficiency with which light is absorbed is comparable for both material pairs, given the prescribed layer thicknesses. Given the similarity in the extent to which these bilayers absorb light, and given that P(NDI2OD-T2) is reported to have a higher electron mobility (0.45−0.85 cm^2/(V s)),[31] compared to PCBM, we were initially surprised that the J_{sc} value of the P3HT/P(NDI2OD-T2) bilayer device (green triangles; Figure 4b) is ∼4 times lower than that of the P3HT/PCBM bilayer device (green triangles; Figure 4a). The external quantum efficiency (EQE) spectra for both devices are shown in the bottom of Figure 4c. Consistent with the device characteristics shown in Figures 4a and 4b, the maximum EQE of the P3HT/PDNI bilayer solar cell is ∼4 times lower than that of the P3HT/PCBM bilayer device. These spectra also indicate that a non-negligible portion of the excitons is generated in the electron acceptor layers, given the similarity between the EQE spectra at lower wavelengths and the UV−vis−NIR spectra of the electron acceptors.[40] This observation likely stems from the fact that the electron acceptor layers are closer to the illumination source, compared to the P3HT layers in these bilayer devices (illumination occurs from the bottom and the electron acceptor comprises the bottom layer of these devices). Given that electron transport is not likely the bottleneck for device operation in the P3HT/P(NDI2OD-T2) bilayer solar cells, we surmise that charge separation at the interface of P3HT/P(NDI2OD-T2) is less efficient than that at the interface of P3HT/PCBM, likely because of morphological differences. Detailed characterization of the extent of phase separation is complicated; attempts are currently underway.

4. Conclusions

With soft-contact lamination (ScL), we have been able to construct and deconstruct organic solar cells for testing

and subsequent characterization, respectively. This process allows device components to be individually, and potentially differently, processed before they are brought into physical contact, effectively obviating the need for the traditional layer-by-layer approach of device fabrication. Testing of bulk-heterojunction organic solar cells with laminated electrodes, as well as bilayer organic solar cells with laminated polymer electron donors, indicate ScL to be robust; efficient electrical contact is established across the laminated interface. Most excitingly, ScL is reversible; the laminated components can be removed after device testing to show the once-buried charge separation interface for structural characterization. From a scientific perspective, ScL affords new opportunities to understand and control interfaces that limit charge separation, since device components can now be individually laminated, removed, and relaminated. From a technological perspective, ScL represents a transformative platform for constructing organic devices and provides a venue for the systematic testing of new materials.

Acknowledgment. This work is supported by the Photovoltaics Program at ONR (No. N000140811175) and a Sloan Research Fellowship to Y.-L.L. Partial funding from an NSF-sponsored MRSEC through the Princeton Center for Complex Materials (No. DMR-081960) is also acknowledged. J.B.K. and Y.S.K. also thank KOSEF (No. 2010-0000378) for partial support. Portions of this research were carried out at the Stanford Synchrotron Radiation Lightsource, which is a national user facility operated by Stanford University on behalf of the U.S. Department of Energy, Office of Basic Energy Sciences.